Journal of Hazardous Materials 459 (2023) 132031

Contents lists available at ScienceDirect

Journal of Hazardous Materials

journal homepage: www.elsevier.com/locate/jhazmat

Surface imprinted-covalent organic frameworks for efficient solid-phase extraction of fluoroquinolones in food samples

Li-Hong Su [a,b,c], Hai-Long Qian [a,b,c,d], Cheng Yang [a,b,c], Chuanxi Wang [e], Zhenyu Wang [e], Xiu-Ping Yan [a,b,c,d,*]

[a] State Key Laboratory of Food Science and Resources, Jiangnan University, Wuxi 214122, China
[b] International Joint Laboratory on Food Safety, Jiangnan University, Wuxi 214122, China
[c] Institute of Analytical Food Safety, School of Food Science and Technology, Jiangnan University, Wuxi 214122, China
[d] Key Laboratory of Synthetic and Biological Colloids, Ministry of Education, Jiangnan University, Wuxi 214122, China
[e] Institute of Environmental Processes and Pollution control, and School of Environment and Civil Engineering, Jiangnan University, Wuxi 214122, China

HIGHLIGHTS

- A novel molecularly imprinted COF (MI-COF) was designed for FQs extraction.
- The prepared MI-COF gave a better adsorption capacity and faster kinetics.
- The multiple imprinted sites of MI-COF allowed selective extraction.
- The MI-COF-HPLC method was sensitive and practical for FQs in food samples.

GRAPHICAL ABSTRACT

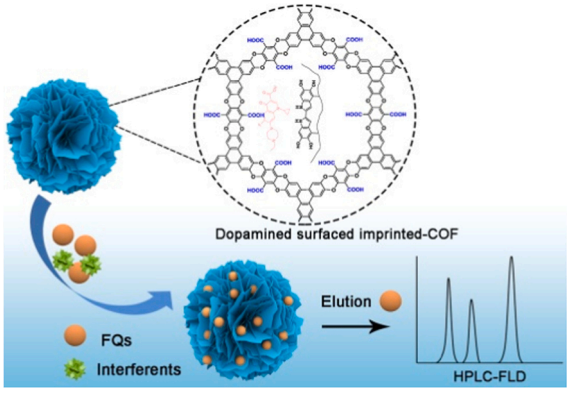

ARTICLE INFO

Editor: Anett Georgi

Keywords:
Covalent organic frameworks
Molecularly imprinted polymers
Solid-phase extraction
Fluoroquinolones

ABSTRACT

Molecularly imprinting on covalent organic frameworks (MI-COF) is a promising way to prepare selective adsorbents for effective extraction of fluoroquinolones (FQs). However, the unstable framework structure and complex imprinting process are challenging for the construction of MI-COF. Here, we report a facile surface imprinting approach with dopamine to generate imprinted cavities on the surface of irreversible COF for highly efficient extraction of FQs in food samples. The irreversible-linked COF was fabricated from hexahydroxytriphenylene and tetrafluorophthalonitrile to ensure COF stability. Moreover, the introduction of dopamine surface imprinted polymer into COF provides abundant imprinted sites and endows excellent selectivity for FQs recognition against other antibiotics. Taking enrofloxacin as a template molecule, the prepared MI-COF gave an exceptional adsorption capacity of 581 mg g^{-1}, a 2.2-fold enhancement of adsorption capacity compared with nonimprinted COF. The MI-COF was further explored as adsorbent to develop a novel solid-phase extraction method coupled with high-performance liquid chromatography for the simultaneous determination of

* Corresponding author at: State Key Laboratory of Food Science and Resources, Jiangnan University, Wuxi 214122, China.
E-mail address: xpyan@jiangnan.edu.cn (X.-P. Yan).

https://doi.org/10.1016/j.jhazmat.2023.132031
Received 23 May 2023; Received in revised form 5 July 2023; Accepted 9 July 2023
Available online 10 July 2023

enrofloxacin, norfloxacin and ciprofloxacin. The developed method gave the low limits of detection at 0.003–0.05 ng mL^{-1}, high precision with relative standard deviations less than 3.5%. The recoveries of spiked FQs in food samples ranged from 80.4% to 110.7%.

1. Introduction

Fluoroquinolones (FQs) are effective antibacterial drugs in animal husbandry and aquaculture industry [14,26]. Ciprofloxacin (CIP), enrofloxacin (ENR) and norfloxacin (NOR) are the most widely used FQs in current veterinary medicine and clinical practice [25,32,38]. However, the increase of excess uptake and illegal abuse leads to serious damage to ecology and organisms [9,43]. Thus, FQs have been restricted as a feed additive while the maximum residual limits have been established in USA, European Union and China [29,30,42]. To ensure food safety, it is important to develop a sensitive and precise detection method for monitoring FQs. However, the low concentration of FQs and contrarily huge content of other interference matrices (matrices with high fat, protein, or sugar content) necessitate an effective pretreatment procedure for food samples prior to instrumental analysis. Solid-phase extraction, liquid-liquid extraction and solid-phase microextraction are often used for this purpose [1,27,33,34,41,44,5,6].

The emerging covalent organic frameworks (COFs) with highly order porous channels, large surface areas and abundant active sites have received great attention for sample pretreatment in the past decade [7, 17–19,24]. COFs, which are covalently connected organic building blocks, adopt two- or three-dimensional structures with highly tunable composition and function [22,35]. Depending on targets, various functional sites can be introduced into COFs via direct polymerization and post-modification strategies to enhance interaction with target molecules [31,39,40,47,54]. COFs could interact with the fluorine sites, benzene ring and other functional groups of FQs by introducing carboxyl, sulfonic acid and metal ions [15,36,4]. However, these functional COFs gave limited selectivity to FQs based on one or nonspecific interactions such as electrostatic attraction, hydrogen bonding, $\pi - \pi$ and van der Waals interactions. As such, the selectivity of COFs in molecular recognition is limited and easily disturbed by complex sample matrixes.

Introducing molecularly imprinted polymers (MIPs) to COFs provide an effective way to improve the specific recognition and extraction selectivity. MIPs are formed based on a “lock and key” mechanism, and able to match a specific type of templates in size, shape and functional groups.[2,45] Recently, a uniform morphology of molecularly imprinted COF (MI-COF) was fabricated with aminopropyltriethoxysilane as functional monomer and tetraethyl orthosilicate as crosslinking agent for selective enrichment of sterigmatocystin [16]. In addition, a carbazole-based MI-COF was prepared with COF as the fluorescence core and bulk-polymerized MIPs as the shell for selective optosensing of ethyl carbamate [12]. A MI-COF@SiO_2 was also synthesized with COF building blocks as functional monomers and cross-linkers for selective extraction of nonsteroidal anti-inflammatory drugs [20]. The above MI-COFs have shown significant improvement in selectivity to targets [12,16,20]. However, the synthesis procedures are relatively complex as cross-linking agent, coupling agent and initiating agent should be used and anaerobic environment should be involved. Furthermore, the dynamic skeleton structure of COFs is easy to deform, and the crystallinity and porosity of COF are hard to retain during the preparation of MI-COFs [46]. More seriously, the collapse of imprinted sites makes MI-COFs lose specific recognition ability.

Dopamine provides an ideal integration of functional monomer and cross-linker to produce imprinted polydopamine (PDA) layer on the surface of organic and inorganic materials. Dopamine can be self-polymerized to PDA in weak alkaline solution without the need for complex instruments or harsh experimental conditions [52]. PDA possesses numbers of amino and phenolic hydroxy groups to provide a certain basis for the specific recognition of targets [50]. Thus, dopamine is attractive for the preparation of MIPs [3,13,49,51]. For instance, molecularly imprinted PDA layer was fabricated on a metal–organic framework-53(Fe) for selective fluorescence detection of metronidazole [51]. Additionally, imprinted PDA layer on the surface of PDA nanospheres was also reported for selective recognition of *pseudomonas aeruginosa* [49].

Herein, we report the fabrication of molecularly imprinted PDA layer on the surface of COF via self-polymerization of dopamine for selective extraction of FQs in food samples. COF-316 is employed as a model COF as its irreversible dioxin linkages endows stable framework to withstand further functional modification [48]. Meanwhile, the cyan group in COF-316 is hydrolyzed to carboxyl groups as binding sites for the interaction with the amino group of dopamine and the adsorption of FQs. In addition, the combination of molecular imprinting with self-polymerization of dopamine produces molecularly imprinted PDA layer on the surface of COF-316 for fast and selective recognition FQs. This work provides a promising method for the fabrication of MIP on COFs for selective extraction of FQs in food samples.

2. Experimental

2.1. Materials and chemicals

ENR, CIP and NOR (99.8%) were purchased from ANPEL laboratory technologies Co., Ltd. (Shanghai, China). Flumequine (FLU), sulfamethoxazole (SMZ) and chloramphenicol (CAP) were purchased from Macklin Biochemical Co., Ltd. (Shanghai, China). 2,3,6,7,10,11-Hexahydroxytriphenylene (HHTP, 95%) and tetrafluorophthalonitrile (TFPN, 98%) were purchased from Jilin Chinese Academy of Sciences-Yanshen Technology Co., Ltd. (Jilin, China). 1,4-dioxane, triethylamine (Et_3N), tetrahydrofuran, sodium hydroxide (NaOH), hydrochloric acid (HCl), acetonitrile (ACN), formic acid (FA), methanol and dopamine were obtained from Aladdin Chemistry Co., Ltd. (Shanghai, China). Ultrapure water from Wahaha Co., Ltd (Hangzhou, China) was used throughout the work.

2.2. Instrumentation

Scanning electron microscope (SEM) images were taken on an SU8100 electron microscope (Hitachi, Japan). Fourier transform infrared (FT-IR) spectra were recorded on a Nicolet IRIS10 spectrometer (Quantachrome, USA). Brunauer-Emmett-Teller (BET) surface area was measured on Autosorb-IQ (Quantachrome, USA) using N_2 adsorption at 77 K. Powder X-ray diffraction (PXRD) patterns were obtained on an X-ray diffractometer equipped with graphite-monochromatized Cu Kα radiation. Zeta-potential was determined on Zetasizer nano ZS (Malvern instruments, Britain). UV–vis absorption spectra were acquired on a UV-3600 PLUS spectrophotometer (Shimadzu, Japan). High-performance liquid chromatography (HPLC) experiments were performed on Waters e2695 HPLC fitted with a fluorescence detector (FLD) and a C18 column (XBridge® C18 5 μm, 4.6 × 250 mm) (Waters, Milford, MA).

2.3. Synthesis of carboxyl functionalized COF-316 (COF-316-COOH)

COF-316 was prepared based on a reported method with slight modification [48]. In brief, 0.0928 mol of HHTP, 0.138 mol of TFPN, 0.56 mol of triethylamine and 2 mL of 1,4-dioxane were added in a Pyrex tube and degassed by three freeze-pump-thaw cycles. Then, the Pyrex tube was placed in an oil bath at 120 ℃ for 3 days. The solid

product was exhaustively washed by tetrahydrofuran and dried under vacuum at 60 °C for overnight.

For the preparation of COF-316-COOH, 100 mg of COF-316 was added into 50 mL 20% NaOH solution (H_2O: ethanol = 1:1) and heated up to 120 °C with condensation reflux for 3 days. Upon cooling to room temperature, the product was washed with deionized water. Then, the precipitate was redispersed in 50 mL 1 M HCl solution and heated up to 120 °C with refluxed. After 2 h, the final product was washed with ultrapure water and dried overnight.

2.4. Synthesis of MI-COF and non-imprinted COF (NI-COF)

MI-COF and NI-COF were synthesized via self-polymerization of dopamine. 20 mg of COF-COOH and 10 mg of ENR was added into 10 mL Tris HCl (10 mM, pH 8.0) under stirring for 2 h. Then, 10 mg of dopamine was added into the mixture and stirred for 5 h. Finally, the resultant composite was washed with methanol-acetic acid (70:30, v/v) to remove template molecules ENR until no UV–vis adsorption. In a parallel, NI-COF was synthesized in the same way but without the addition of template molecules.

2.5. Adsorption experiments

To study adsorption kinetics, 1 mg of MI-COF or NI-COF was dispersed in 4 mL 50 mg L^{-1} of ENR solution. After shaking for a designated period, the sample solution was separated on 0.2 μm hydrophilic nylon syringe filter to remove all the suspended MI-COF or NI-COF. The residual ENR in the supernatant was then analyzed by UV–vis spectrometry. The pseudo-first-order kinetics and pseudo-second-order kinetics was calculated according to Eq. (1) and (2), respectively.

$$\ln(q_e - q_t) = \ln q_e - K_1 t \quad (1)$$

$$\frac{t}{q_t} = \frac{1}{K_2 q_e^2} + \frac{1}{q_e} t \quad (2)$$

where q_t and q_e are the adsorption capacity (mg g^{-1}) at time t and equilibrium time, respectively. K_1 and K_2 are the adsorption rate constant (g mg^{-1} min^{-1}) of pseudo-first-order kinetics and pseudo-second-order kinetics, respectively.

For adsorption isotherm study, 1 mg of MI-COF or NI-COF was dispersed in 4 mL different of ENR solution (60–300 mg mL^{-1}). The mixture was shaken at room temperature for 120 min, and then filtered through a 0.2 μm hydrophilic nylon syringe filter. The residual ENR in the supernatant was analyzed by UV–vis spectrometry. The Langmuir and Freundlich adsorption isotherms were expressed according to the following equation:

$$\frac{C_e}{q_e} = \frac{C_e}{q_{max}} + \frac{1}{q_{max} K_L} \quad (3)$$

$$\ln q_e = \ln K_F + \frac{1}{n} \ln C_e \quad (4)$$

where q_{max} is the maximum adsorption capacity of adsorbent (mg g^{-1}) and K_L is the Langmuir constant (L mg^{-1}). q_e (mg g^{-1}) and Ce (mg L^{-1}) are the equilibrium adsorption capacity and equilibrium concentration of ENR, respectively. K_F is the Freundlich constant (L mg^{-1}).

The selective recognition ability of MI-COF and NI-COF was subsequently assessed by comparing the adsorbed amount of ENR and its structural analogues such as NOR, CIP, FLU, SMZ and CAP. Specifically, 1 mg of MI-COF or NI-COF was dispersed in 4 mL of ENR or analogues (100 mg mL^{-1}) and shaken at 150 rpm. The residual sample solution in the supernatant was analyzed by UV–vis spectrometry.

2.6. Procedures for dispersed solid-phase extraction and analysis

Briefly, 0.5 mg of MI-COF was added into 16 mL of FQs antibiotic standard solution or sample solution with a certain concentration. After shaking for 8 min, MI-COF was collected by centrifugation and then eluted with 2 mL of acetonitrile containing 40% formic acid. The FQs in the desorption solution was determined by HPLC-FLD on an analytical C18 column. A mixture of 0.1% formic acid and acetonitrile (81:19, V/V) was used as the mobile phase at a flow rate was 0.8 mL min^{-1}. The excitation and emission wavelengths for fluorescence detector were 280 nm and 450 nm, respectively.

2.7. Application of food sample analysis

Chicken, fish, shrimp and pork samples were bought from the local supermarket (Wuxi, China). The edible part of samples was chopped and homogenized for further extraction. Subsequently, 5 g of sample was added to 20 mL of acidulated acetonitrile and vortexed for 30 s. After ultrasound for 20 min, the mixture was centrifuged at 10000 rpm and the supernatant was collected, and repeated once. All the collected sample solution was dried with a nitrogen stream. The residue was dissolved with 200 μL methanol and made up to 16 mL with ultrapure water for subsequent dispersed solid-phase extraction and analysis.

3. Results and discussion

3.1. Design, preparation and characterization of MI-COF

Fig. 1 shows the design and preparation of MI-COF. Firstly, HHTP and TFPN were used as the building monomers to synthesize irreversible COF-316 through a solvothermal reaction [48]. Owing to the strong robustness of dioxin rings, the resultant COF-316 provides exceptional stability in harsh environments [48]. COF-316-COOH was prepared from COF-316 via a hydrolysis reaction to provide a large number of binding sites for the adsorption of target via multiple interactions. ENR was selected as template molecule as it possesses a large portion of similar molecular structure to NOR and CIP but larger molecular size than NOR and CIP (Fig. S1), so that the prepared MI-COF can effectively extract NOR and CIP too. Dopamine was then used as both functional monomer and cross-linking reagent to produce adherent PDA layer on the surface of ENR-adsorbed COF-316-COOH. Removing the template molecules gave MI-COF having abundant recognition cavities with specific geometry and size for selective extraction of the target from complex samples.

The highly crystalline dioxin-linked COF-316 was obtained with 156 μL of Et_3N (Fig. S2). The as-prepared COF-316 exhibited an intense peak at 4.2° and other minor peaks at 8.4° and 27.1°, which are ascribed to the (100), (210) and (001) planes, respectively [10]. No obvious change in the PXRD pattern of COF-316 under different chemical environments indicates the good stability of COF-316 (Fig. S3). Moreover, carboxyl functionalization did not lead to an obvious change in the PXRD pattern of COF-316-COOH, indicating the high stability of COF-316 (Fig. 2 A). The construction of COF-316 and COF-316-COOH were further verified by FT-IR spectroscopy (Fig. S4). The characteristic bands for the dioxin C-O asymmetric stretching at 1020 cm^{-1} and symmetric stretching at 1266 cm^{-1}, as well as the appearance of a -CN stretching band at 2238 cm^{-1} and the decrease -OH stretching band at 3420 cm^{-1} compared to HHTP monomer further confirm the successful synthesis of COF-316 [23]. The appearance of a C═O stretching peak at 1718 cm^{-1} and the disappearance of -CN band at 2240 cm^{-1} confirm the conversion from cyano to carboxyl groups [55]. In addition, the conversion from cyano to carboxyl groups also made the zeta potential an obvious change from − 1.87 mV to − 34.87 mV due to a large amount of electronegative -COOH group (Fig. 2B). All the above results indicate the successful synthesis of COF-316-COOH.

The morphology of the prepared materials was characterized by SEM

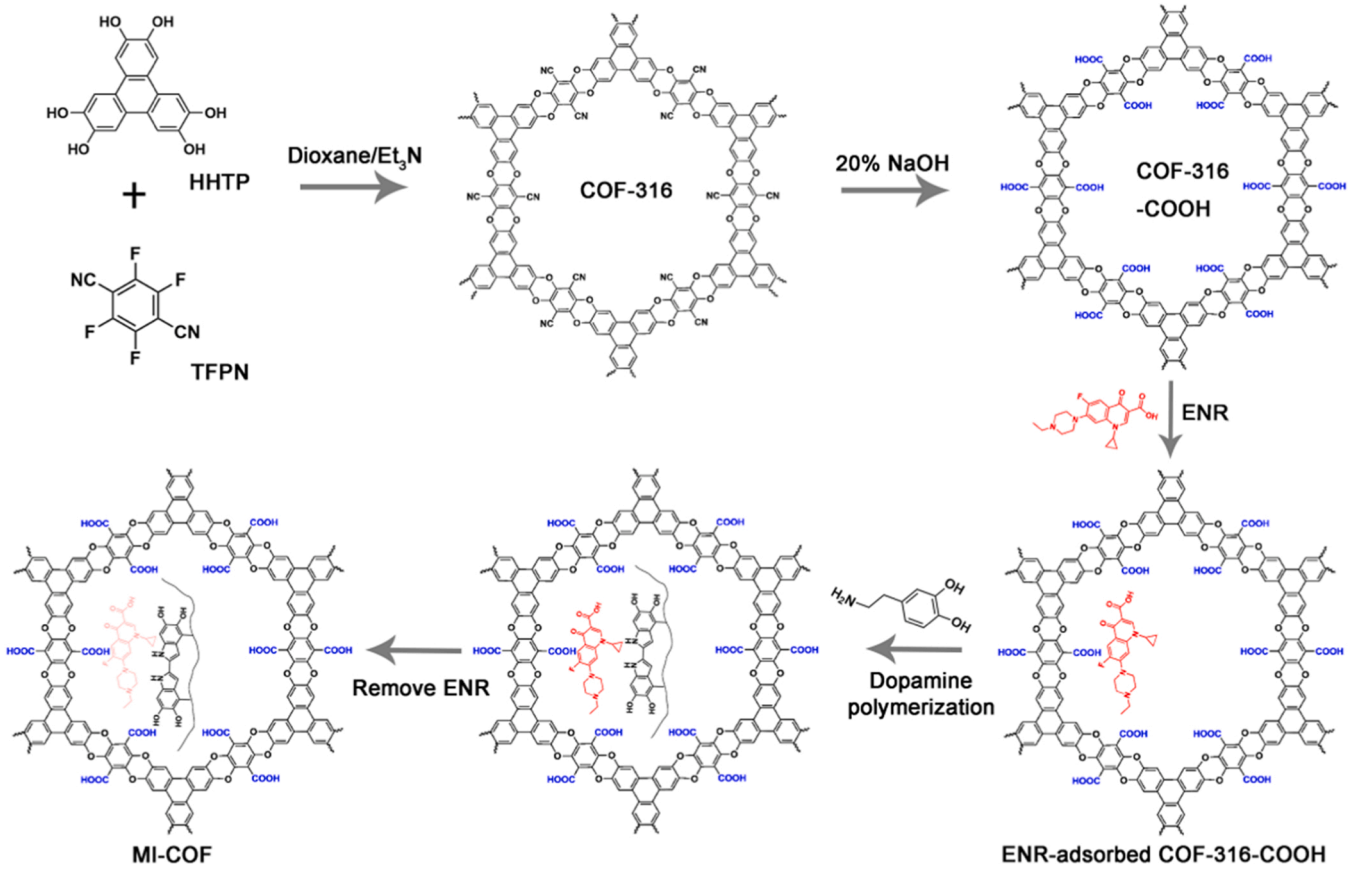

Fig. 1. Illustration for the synthesis of COF-316-COOH and MI-COF.

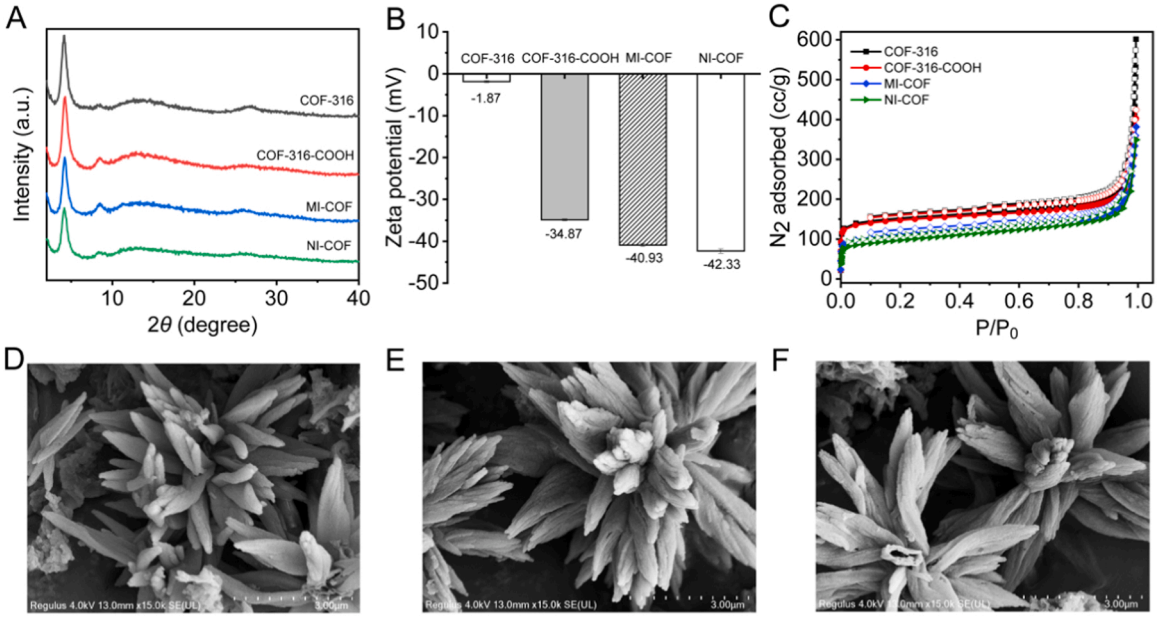

Fig. 2. (A) PXRD patterns of COF-316, COF-316-COOH, MI-COF and NI-COF. (B) Zeta potential of COF-316, COF-316-COOH, MI-COF and NI-COF. (C) N_2 adsorption-desorption isotherms of COF-316, COF-316-COOH, MI-COF and NI-COF. SEM images of (D) COF-316-COOH, (E) MI-COF and (F) NI-COF.

(Fig. 2D-F). COF-316-COOH gave fusiform-like morphology with a relatively smooth surface. MI-COF and NI-COF were still fusiform like, but thicker and rougher than COF-316-COOH, suggesting the successful polymerization of PDA. Moreover, MI-COF and NI-COF displayed the same PXRD pattern as COF-316-COOH, but lower peak intensity, demonstrating the stable crystal structure of COF after of PDA polymerization and molecular imprinting (Fig. 2 A). MI-COF and NI-COF produced a negative surface charge due to the deposition of PDA (Fig. 2B). The BET surface areas for COF-316, COF-316-COOH, MI-COF and NI-COF were 581.6, 561.3, 408.4 and 354.7 $m^2\ g^{-1}$, respectively

(Fig. 2 C). MI-COF gave a larger surface area than NI-COF due to a large number of imprinted cavities. Furthermore, MI-COF showed a wider pore-size distribution around 1.5 nm closing to the size of template ENR for facile ENR access, while NI-COF exhibited a narrower pore-size distribution around 1.1 nm (Fig. S1 and S5).

3.2. Optimization of MI-COF synthesis

The amount of ENR and dopamine were adjusted to give the best imprinting efficiency of MI-COF. The adsorption capacity of MI-COF increased as the amount of ENR increased up to 10 mg, then unchanged with further increase of the amount of ENR (Fig. S6A). Dopamine as functional monomer and cross-linking agent can adhere to COF-316-COOH surface. Excessive dopamine not only reduced the number of imprinted cavity but also increased the self-aggregation of dopamine. So, the effectiveness of molecular imprinting was affected by the amount of dopamine. The imprinting factor is defined as the ratio of the adsorption capacity of MI-COF to NI-COF to assess imprinting efficiency. The imprinting factor increased with the amount of dopamine from 5 to 10 mg, changed slightly after 10 mg (Fig. S6B). Therefore, 10 mg of ENR and dopamine were used to prepare MI-COF.

3.3. Adsorption performance of MI-COF

Taking ENR as a model analyte, the adsorption performance was investigated based on MI-COF and NI-COF. The adsorption kinetics of ENR (50 mg L^{-1}) was examined at room temperature. MI-COF displayed an initial sharp uptake within 1 min, and the adsorption equilibrium was achieved after 5 min, reflecting a fast ENR adsorption process (Fig. 3 A). However, NI-COF needed 20 min to reach the adsorption equilibrium. The adsorption followed a pseudo-second-order kinetics (Fig. 3B and S7A; Table S1), indicating that the adsorption process toward ENR was mainly predominated by chemisorption [8]. MI-COF showed a faster adsorption process than NI-COF due to the specific recognition sites and efficient mass transfer of MI-COF.

The adsorption isotherm experiments were carried out with varied initial ENR concentrations to further evaluate adsorption capacity (Fig. 3 C). The equilibrium adsorption capacity of MI-COF showed an obvious increase in the range of 60–175 mg L^{-1} ENR due to a large number of imprinted pores available in MI-COF. MI-COF almost reached the adsorption saturation with further increase of ENR concentration because the imprinted pores were completely occupied by ENR. However, NI-COF showed adsorption saturation over 100 mg L^{-1} ENR. Moreover, the maximum ENR adsorption capacity of MI-COF

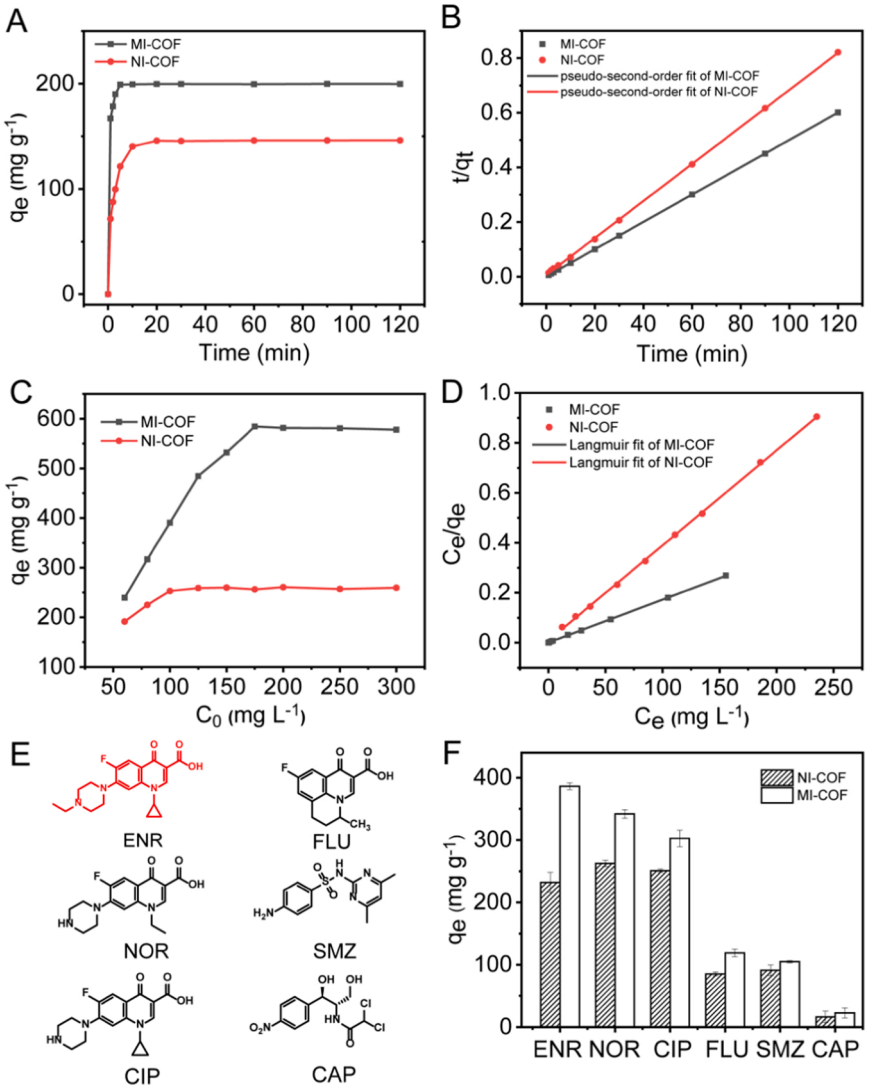

Fig. 3. (A) Adsorption kinetics curves of MI-COF and NI-COF. (B) Pseudo-second-order fitting plots of MI-COF and NI-COF. (C) Adsorption isotherms of MI-COF and NI-COF. (D) Langmuir isotherm plots of MI-COF and NI-COF. (E) Chemical structure of ENR, NOR, CIP, FLU, SMZ and CAP. (F) Adsorption selectivity of MI-COF and NI-COF for ENR, NOR, CIP, FLU, SMZ and CAP.

(581 mg g^{-1}) is 2.2 times that of NI-COF (262 mg g^{-1}). The adsorption process of MI-COF and NI-COF followed the Langmuir isothermal adsorption model (Fig. 3D and S7B, Table S2).

Two structurally related FQs and three other kinds of typical antibiotics FLU, SMZ and CAP were selected as interference molecules to reveal the adsorption selectivity of MI-COF. Obviously, MI-COF gave larger adsorption capacity for ENR than the studied interference molecules (Fig. 3 F). The selectivity imprinting factors, defined as the ratio of the adsorption capacity of template to other molecules, were 1.1, 1.3, 3.2, 3.7 and 16 for NOR, CIP, FLU, SMZ and CAP, respectively. The selective imprinting factors of MI-COF toward NOR and CIP are quite small owing to the similar chemical structures (Fig. 3E). In comparison, the selective imprinting factors of MI-COF toward other three interference molecules FLU, SMZ and CAP are much higher as it is difficult for these molecules to match the recognition cavities and specific recognition groups of ENR. As such, MI-COF gave a lower adsorption capacity for FLU, SMZ and CAP. Therefore, the prepared MI-COF is promising for simultaneous extraction of ENR, NOR and CIP in real samples.

3.4. Adsorption mechanism

The prepared MI-COF provides a large number of specific recognition sites and cavities for the recognition of ENR. MI-COF and ENR have abundant benzene ring structure for π–π interaction. At the same time, the abundant hydroxyl and carboxyl sites in MI-COF provide hydrogen bonding and electrostatic interaction with ENR (Fig. 4 A). UV–vis spectroscopy, FT-IR spectroscopy and Zeta potential were further analyzed to confirm the adsorption mechanism of MI-COF toward ENR. ENR adsorption led to a red shift from 271 nm to 273 nm in UV–vis spectra due to the π–π interaction between MI-COF and ENR (Fig. 4B) [20,21,53]. The characteristic peak of aromatic ring stretching on MI-COF shifted from 1517 cm^{-1} to 1513 cm^{-1} in FT-IR spectra (Fig. 4 C), indicating π−π interaction for the adsorption of ENR. Meanwhile, the characteristic dioxin C-O asymmetric bands at 1266 cm^{-1} and 1020 cm^{-1} in MI-COF shifted to 1260 cm^{-1} and 1017 cm^{-1}, respectively, owing to the hydrogen bonding [10,15]. In addition, the surface of MI-COF maintained negative charge in the pH range from 3 to 11 (Fig. 4D). After ENR adsorption, the surface zeta potential of MI-COF increased owing to the electrostatic interaction between the charged amino group of piperazinyl ring in ENR and the negative charge of MI-COF [11,28,37].

3.5. Optimization of MI-COF based solid-phase extraction

Key experimental parameters, including extraction time, sample pH, type of eluent and desorption time were optimized to give the superior efficiency of MI-COF for the extraction of three typical FQs ENR, NOR and CIP. An extraction time of 8 min was sufficient for the extraction of ENR, NOR and CIP (Fig. 5A). A sample pH of 6 gave the maximum recoveries for the extraction of the FQs (Fig. 5B). Proper elution solvent is quite significant to guarantee the full desorption of targets. It was found that the use of a mixture of ACN and formic acid (60:40 v/v) as the elution solvent for 10 min desorption gave the best desorption of the adsorbed the FQs (Fig. 5C and D).

3.6. Analytical performance

The prepared MI-COF was employed as the adsorbent for solid-phase extraction coupled with HPLC-FLD for the determination of FQs. The figures of merit for the developed method, including linear ranges, determination coefficients (R^2), limits of detection (LODs, S/N = 3) and limits of quantitation (LOQs, S/N = 10), are summarized in Table 1. The developed method gave excellent linear calibration plots ($R^2 > 0.998$) with a wide linear range of 0.01 (ENR) or 0.1 (NOR and CIP)–1000 ng mL^{-1}. In addition, the LODs and LOQs were 0.003 (ENR)–0.05 (NOR and CIP) and 0.01 (ENR)–0.16 (NOR and CIP) ng mL^{-1}, respectively. The relative standard deviations (RSD, $n = 5$) for intraday and interday determination of FQs at 25 ng mL^{-1} were in the range of 2.2–2.8% and 2.9–3.5%, respectively. Compared with previously reported methods for FQs, the developed method has wider linearity and lower LODs (Table S3). In addition, the prepared MI-COF possessed good recyclability because of only a slight reduction in extraction capacity

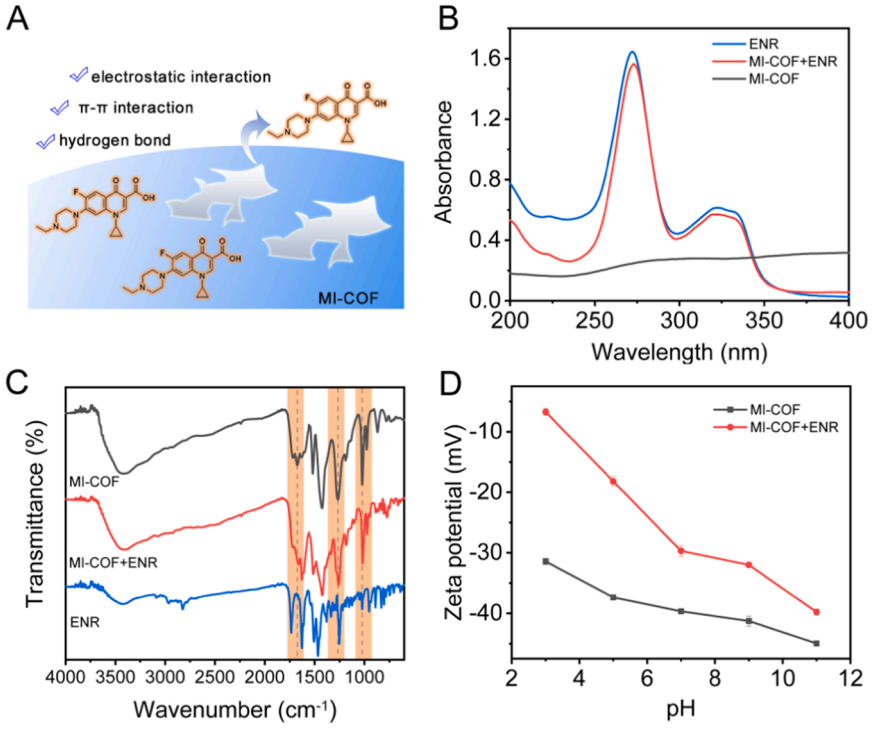

Fig. 4. (A) Illustration of the mechanism for selective adsorption of ENR on MI-COF. (B) UV–vis spectroscopy of ENR, MI-COF before and after the adsorption of ENR. (C) FT-IR spectroscopy of ENR, MI-COF before and after the adsorption of ENR. (D) Zeta potentials of MI-COF at different pH after ENR adsorption.

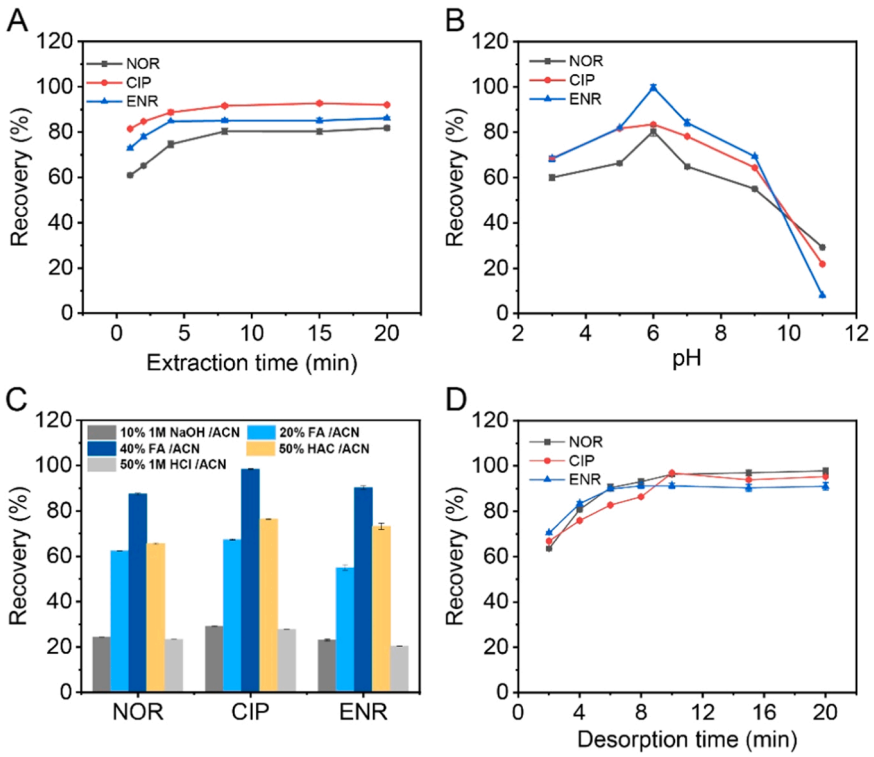

Fig. 5. Optimization of extraction and desorption parameters: (A) Extraction time. (B) pH of sample solution. (C) Desorption solvent. (D) Desorption time.

Table 1
Figures of merit of the developed method for the determination of FQs.

Analyte	Linear range (ng mL^{-1})	R^2	LODs (ng mL^{-1})	LOQs (ng mL^{-1})	RSD (%)	
					Intraday ($n = 5$)	Interday ($n = 5$)
NOR	0.1–1000	0.9980	0.02	0.07	2.7	3.5
CIP	0.1–1000	0.9999	0.05	0.16	2.8	3.1
ENR	0.01–1000	0.9993	0.003	0.01	2.2	2.9

and a good retention of the PXRD pattern of MI-COF after six cycles (Fig. S8).

3.7. Food sample analysis

The developed method was further applied to the determination of FQs residues in food samples including chicken, fish, shrimp and pork. Only NOR and ENR in the fish sample were found to be 6.4 μg kg^{-1} and 13.9 μg kg^{-1}, respectively. However, no the studied FQs in the chicken, shrimp and pork samples were found. Subsequently, these samples with spiked various concentrations of FQs (25, 50 and 100 μg kg^{-1}) were analyzed to validate the proposed method (Table 2). The recoveries were found to be 80.4%–110.7%, implying a good potential of the developed method in the analysis food samples for the FQs.

Table 2
Analytical results for the determination of FQs in food samples (mean ± s, n = 5).

Samples	Spiked analyte (μg kg^{-1})	NOR		CIP		ENR	
		determined (μg kg^{-1})	recovery (%)	determined (μg kg^{-1})	recovery (%)	determined (μg kg^{-1})	recovery (%)
chicken	0	ND[a]	-	ND[a]	-	<LOQ	-
	25	20.6 ± 1.3	82.4 ± 5.2	24.5 ± 0.8	83.2 ± 3.3	23.8 ± 0.8	98.2 ± 3.4
	50	45.8 ± 0.7	91.5 ± 1.4	48.2 ± 0.6	96.5 ± 1.1	51.1 ± 0.9	102.2 ± 1.7
	100	80.8 ± 1.4	80.8 ± 1.4	84.4 ± 1.9	84.4 ± 1.9	87.3 ± 1.3	87.3 ± 1.3
fish	0	6.4 ± 0.3	-	ND[a]	-	13.9 ± 0.1	-
	25	22.7 ± 0.3	91.5 ± 1.2	25.2 ± 0.5	100.7 ± 1.8	27.5 ± 1.6	110.1 ± 6.3
	50	47.7 ± 1.2	95.4 ± 2.5	46.9 ± 0.8	93.9 ± 1.7	47.5 ± 1.6	94.9 ± 3.2
	100	82.9 ± 2.6	82.9 ± 2.6	96.4 ± 2.4	96.4 ± 2.4	102.8 ± 1.7	102.8 ± 1.7
shrimp	0	ND[a]	-	ND[a]	-	ND[a]	-
	25	20.9 ± 0.5	83.5 ± 2.1	25.6 ± 0.8	102.4 ± 3.1	24.7 ± 0.5	98.9 ± 2.2
	50	41.1 ± 1.8	82.2 ± 3.6	43.6 ± 0.7	87.3 ± 1.3	46.7 ± 1.7	93.4 ± 3.3
	100	80.4 ± 1.4	80.4 ± 1.4	104.9 ± 6.5	104.9 ± 6.5	104.3 ± 3.1	104.3 ± 3.1
pork	0	ND[a]	-	ND[a]	-	<LOQ	-
	25	22.6 ± 0.5	90.3 ± 3.8	21.1 ± 0.5	84.5 ± 2.1	27.7 ± 0.1	110.7 ± 0.4
	50	41.9 ± 0.6	83.7 ± 1.2	48.5 ± 1.9	97.1 ± 3.9	47.9 ± 1.5	95.9 ± 2.9
	100	81.3 ± 7.6	81.3 ± 7.6	98.6 ± 1.4	98.6 ± 1.4	103.2 ± 1.1	103.2 ± 1.1

[a] not detected

4. Conclusion

We have reported the fabrication of a novel adsorbent MI-COF via a facile surface imprinting approach with dopamine to generate imprinted cavities on the surface of irreversible COF for effective extraction of FQs in food samples. The combination of dopamine surface imprinted polymer and irreversible linked-COF structure gives many advantages including large surface area to provide imprinting sites, high selectivity, good stability, and facile synthesis and fast adsorption kinetics. On the basis of MI-COF, we have also developed a solid-phase extraction coupled with HPLC-FLD method for highly sensitive and selective determination of FQs in food samples. This work provides a simple method to fabricate MI-COF for solid-phase extraction of FQs in complex samples.

Environmental implications

Fluoroquinolones (FQs) antibiotics are effective antibacterial drugs in animal husbandry and aquaculture industry worldwide, but the increase of excess uptake and illegal abuse leads to serious damage to environment, ecology and organisms. This work reported the fabrication of a novel adsorbent MI-COF via a facile surface imprinting approach with dopamine to generate imprinted cavities on the surface of irreversible COF for effective extraction of FQs in food samples. The developed method is of great significance for selective monitoring trace residues of FQs in environmental samples.

CRediT authorship contribution statement

Li-Hong Su: Methodology, Validation, Data curation, Investigation, Writing – original draft preparation. **Hai-Long Qian**: Validation, Investigation. **Cheng Yang**: Methodology, Resources. **Chuanxi Wang**: Methodology, Resources. **Zhenyu Wang:** Methodology, Resources. **Xiu-Ping Yan**: Formal analysis, Validation, Writing – review & editing, Conceptualization, Funding acquisition, Project administration.

Declaration of Competing Interest

The authors declare that they have no known competing financial interests or personal relationships that could have appeared to influence the work reported in this paper.

Data availability

Data will be made available on request.

Acknowledgments

Financial supports from the National Natural Science Foundation of China (nos. 22076066 and 22176073), the National First-class Discipline Program of Food Science and Technology (no. JUFSTR 20180301), and the Program of "Collaborative Innovation Center of Food Safety and Quality Control in Jiangsu Province" are highly appreciated.

Appendix A. Supporting information

Supplementary data associated with this article can be found in the online version at doi:10.1016/j.jhazmat.2023.132031.

References

[1] Bayatloo, M.R., Salehpour, N., Alavi, A., Nojavan, S., 2022. Introduction of maltodextrin nanosponges as green extraction phases: magnetic solid phase extraction of fluoroquinolones. Carbohydr Polym 297, 119992. https://doi.org/10.1016/j.carbpol.2022.119992.

[2] BelBruno, J.J., 2018. Molecularly imprinted polymers. Chem Rev 119, 94–119. https://doi.org/10.1021/acs.chemrev.8b00171.

[3] Borchers, A., Pieler, T., 2010. Programming pluripotent precursor cells derived from Xenopus embryos to generate specific tissues and organs. Genes 1, 413–426. https://doi.org/10.3390/genes1030413.

[4] Bu, F., Huang, W., Xian, M., Zhang, X., Liang, F., Liu, X., Sun, X., Feng, D., 2022. Magnetic carboxyl-functionalized covalent organic frameworks for adsorption of quinolones with high capacities, fast kinetics and easy regeneration. J Clean Prod 336, 130485. https://doi.org/10.1016/j.jclepro.2022.130485.

[5] Cai, Z., Zhou, X., Yang, Y., Li, J., Liu, W., Wang, Q., Hao, L., Wang, Z., Yamauchi, Y., You, J., Zhang, S., Wu, Q., Wang, C., 2023. Cyano-functionalized ionic porous polymer: a novel adsorbent for effectively enriching trace estrogens in water and milk. Chem Eng J 466, 143315. https://doi.org/10.1016/j.cej.2023.143315.

[6] Chen, J., Ying, G.G., Deng, W.J., 2019. Antibiotic residues in food: extraction, analysis, and human health concerns. J Agr Food Chem 67, 7569–7586. https://doi.org/10.1021/acs.jafc.9b01334.

[7] Cui, W.R., Zhang, C.R., Jiang, W., Li, F.F., Liang, R.P., Liu, J., Qiu, J.D., 2020. Regenerable and stable sp(2) carbon-conjugated covalent organic frameworks for selective detection and extraction of uranium. Nat Commun 11, 436. https://doi.org/10.1038/s41467-020-14289-x.

[8] Du, Z.-D., Cui, Y.-Y., Yang, C.-X., Yan, X.-P., 2019. Core–shell magnetic amino-functionalized microporous organic network nanospheres for the removal of tetrabromobisphenol a from aqueous solution. ACS Appl Nano Mater 2, 1232–1241. https://doi.org/10.1021/acsanm.8b02119.

[9] Fernandez, F., Pinacho, D.G., Sanchez-Baeza, F., Marco, M.P., 2011. Portable surface plasmon resonance immunosensor for the detection of fluoroquinolone antibiotic residues in milk. J Agr Food Chem 59, 5036–5043. https://doi.org/10.1021/jf1048035.

[10] Guan, X., Li, H., Ma, Y., Xue, M., Fang, Q., Yan, Y., Valtchev, V., Qiu, S., 2019. Chemically stable polyarylether-based covalent organic frameworks. Nat Chem 11, 587–594. https://doi.org/10.1038/s41557-019-0238-5.

[11] Guo, X., Kang, C., Huang, H., Chang, Y., Zhong, C., 2019. Exploration of functional MOFs for efficient removal of fluoroquinolone antibiotics from water. Micro Mesopor Mater 286, 84–91. https://doi.org/10.1016/j.micromeso.2019.05.025.

[12] Han, L., Meng, C., Zhang, D., Liu, H., Sun, B., 2022. Fabrication of a fluorescence probe via molecularly imprinted polymers on carbazole-based covalent organic frameworks for optosensing of ethyl carbamate in fermented alcoholic beverages. Anal Chim Acta 1192, 339381. https://doi.org/10.1016/j.aca.2021.339381.

[13] Han, S., Leng, Q., Teng, F., Ding, Y., Yao, A., 2022. Preparation of mesh covalent organic framework Tppa-2-based adsorption enhanced magnetic molecularly imprinted composite for selective extraction of tetracycline residues from animal-derived foods. Food Chem 384, 132601. https://doi.org/10.1016/j.foodchem.2022.132601.

[14] Jiang, J., Jiang, X., Zou, Y., Zhai, J., Ding, W., Li, H., Zheng, H., 2023. Facile synthesis of acid catalyzed sulfonic acid-amide functionalized magnetic sodium alginate and its efficient adsorption for ciprofloxacin and moxifloxacin. J Clean Prod 391, 136122. https://doi.org/10.1016/j.jclepro.2023.136122.

[15] Jiang, W., Cui, W.R., Liang, R.P., Qiu, J.D., 2021. Difunctional covalent organic framework hybrid material for synergistic adsorption and selective removal of fluoroquinolone antibiotics. J Hazard Mater 413, 125302. https://doi.org/10.1016/j.jhazmat.2021.125302.

[16] Li, C.-Y., Lv, S.-W., Yang, L., Wang, J., Liu, J.-M., Wang, S., 2022. Facile preparation of uniform-sized covalent organic framework nanoflowers as versatile sample-pretreatment platforms for sensitive and specific determination of hazardous substances. J Hazard Mater 438, 129566. https://doi.org/10.1016/j.jhazmat.2022.129566.

[17] Li, J., Wang, Z., Li, J., Zhang, S., An, Y., Hao, L., Yang, X., Wang, C., Wang, Z., Wu, Q., 2022. Novel N-riched covalent organic framework for solid-phase microextraction of organochlorine pesticides in vegetable and fruit samples. Food Chem 388, 133007. https://doi.org/10.1016/j.foodchem.2022.133007.

[18] Li, N., Du, J., Wu, D., Liu, J., Li, N., Sun, Z., Li, G., Wu, Y., 2018. Recent advances in facile synthesis and applications of covalent organic framework materials as superior adsorbents in sample pretreatment. TrAC-Trend Anal Chem 108, 154–166. https://doi.org/10.1016/j.trac.2018.08.025.

[19] Li, S., Liu, W., Wang, Q., Xu, M., An, Y., Hao, L., Wang, C., Wu, Q., Wang, Z., 2022. Constructing magnetic covalent organic framework EB-COF@Fe(3)O(4) for sensitive determination of five benzoylurea insecticides. Food Chem 382, 132362. https://doi.org/10.1016/j.foodchem.2022.132362.

[20] Li, W., Chen, N., Zhu, Y., Shou, D., Zhi, M., Zeng, X., 2019. A nanocomposite consisting of an amorphous seed and a molecularly imprinted covalent organic framework shell for extraction and HPLC determination of nonsteroidal anti-inflammatory drugs. Microchim Acta 186, 76. https://doi.org/10.1007/s00604-018-3187-6.

[21] Li, Y., Yang, C.-X., Qian, H.-L., Zhao, X., Yan, X.-P., 2019. Carboxyl-functionalized covalent organic frameworks for the adsorption and removal of triphenylmethane dyes. ACS Appl Nano Mater 2, 7290–7298. https://doi.org/10.1021/acsanm.9b01781.

[22] Li, Z., He, T., Gong, Y., Jiang, D., 2020. Covalent organic frameworks: pore design and interface engineering. Acc Chem Res 53, 1672–1685. https://doi.org/10.1021/acs.accounts.0c00386.

[23] Li, Z., Zhu, R., Zhang, P., Yang, M., Zhao, R., Wang, Y., Dai, X., Liu, W., 2022. Functionalized polyarylether-based COFs for rapid and selective extraction of uranium from aqueous solution. Chem Eng J 434, 134623. https://doi.org/10.1016/j.cej.2022.134623.

[24] Lohse, M.S., Bein, T., 2018. Covalent organic frameworks: structures, synthesis, and applications. Adv Funct Mater 28, 1705553. https://doi.org/10.1002/adfm.201705553.

[25] Lu, H.-z, Chen, Z.-r, Xu, S.-f, 2022. Surface Molecularly Imprinted Polymers on Multi-Function MnO2-Decorated Magnetic Carbon Nanotubes for Dispersive Solid-Phase Extraction of Three Fluoroquinolones from Milk Samples. ACS Food Sci Tech 2, 1612–1621. https://doi.org/10.1021/acsfoodscitech.2c00218.
[26] Lu, W., Jiao, Y., Gao, Y., Qiao, J., Mozneb, M., Shuang, S., Dong, C., Li, C.Z., 2018. Bright yellow fluorescent carbon dots as a multifunctional sensing platform for the label-free detection of fluoroquinolones and histidine. ACS Appl Mater Interfaces 10, 42915–42924. https://doi.org/10.1021/acsami.8b16710.
[27] Pang, J., Liao, Y., Huang, X., Ye, Z., Yuan, D., 2019. Metal-organic framework-monolith composite-based in-tube solid phase microextraction on-line coupled to high-performance liquid chromatography-fluorescence detection for the highly sensitive monitoring of fluoroquinolones in water and food samples. Talanta 199, 499–506. https://doi.org/10.1016/j.talanta.2019.03.019.
[28] Rodriguez, E., Navarro-Villoslada, F., Benito-Pena, E., Marazuela, M.D., Moreno-Bondi, M.C., 2011. Multiresidue determination of ultratrace levels of fluoroquinolone antimicrobials in drinking and aquaculture water samples by automated online molecularly imprinted solid phase extraction and liquid chromatography. Anal Chem 83, 2046–2055. https://doi.org/10.1021/ac102839n.
[29] Shen, Y., Jia, F., Liang, A., He, Y., Peng, Y., Dai, H., Fu, Y., Wang, J., Li, Y., 2022. Monovalent Antigen-Induced Aggregation (MAA) Biosensors Using Immunomagnetic Beads in Both Sample Separation and Signal Generation for Label-Free Detection of Enrofloxacin. ACS Appl Mater Interfaces 14, 8816–8823. https://doi.org/10.1021/acsami.1c23398.
[30] Speltini, A., Sturini, M., Maraschi, F., Profumo, A., Albini, A., 2011. Analytical methods for the determination of fluoroquinolones in solid environmental matrices. TrAC-Trend Anal Chem 30, 1337–1350. https://doi.org/10.1016/j.trac.2011.04.011.
[31] Sun, Q., Aguila, B., Perman, J., Earl, L.D., Abney, C.W., Cheng, Y., Wei, H., Nguyen, N., Wojtas, L., Ma, S., 2017. Postsynthetically modified covalent organic frameworks for efficient and effective mercury removal. J Am Chem Soc 139, 2786–2793. https://doi.org/10.1021/jacs.6b12885.
[32] Wang, M., Ceto, X., Del Valle, M., 2022. A sensor array based on molecularly imprinted polymers and machine learning for the analysis of fluoroquinolone antibiotics. ACS Sens 7, 3318–3325. https://doi.org/10.1021/acssensors.2c01260.
[33] Wang, Q., Zhang, S., Li, Z., Wang, Z., Wang, C., Alshehri, S.M., Bando, Y., Yamauchi, Y., Wu, Q., 2023. Design of hyper-cross-linked polymers with tunable polarity for effective preconcentration of aflatoxins in grain. Chem Eng J 453, 139544. https://doi.org/10.1016/j.cej.2022.139544.
[34] Wang, Y.F., Wang, Y.G., Ouyang, X.K., Yang, L.Y., 2017. Surface-Imprinted Magnetic Carboxylated Cellulose Nanocrystals for the Highly Selective Extraction of Six Fluoroquinolones from Egg Samples. ACS Appl Mater Interfaces 9, 1759–1769. https://doi.org/10.1021/acsami.6b12206.
[35] Wang, Z., Zhang, S., Chen, Y., Zhang, Z., Ma, S., 2020. Covalent organic frameworks for separation applications. Chem Soc Rev 49, 708–735. https://doi.org/10.1039/c9cs00827f.
[36] Wen, A., Li, G., Wu, D., Yu, Y., Yang, Y., Hu, N., Wang, H., Chen, J., Wu, Y., 2020. Sulphonate functionalized covalent organic framework-based magnetic sorbent for effective solid phase extraction and determination of fluoroquinolones. J Chromatogr A 1612, 460651. https://doi.org/10.1016/j.chroma.2019.460651.
[37] Weng, X., Cai, W., Owens, G., Chen, Z., 2021. Magnetic iron nanoparticles calcined from biosynthesis for fluoroquinolone antibiotic removal from wastewater. J Clean Prod 319, 128734. https://doi.org/10.1016/j.jclepro.2021.128734.
[38] Xiao, R., Wang, S., Ibrahim, M.H., Abdu, H.I., Shan, D., Chen, J., Lu, X., 2019. Three-dimensional hierarchical frameworks based on molybdenum disulfide-graphene oxide-supported magnetic nanoparticles for enrichment fluoroquinolone antibiotics in water. J Chromatogr A 1593, 1–8. https://doi.org/10.1016/j.chroma.2019.02.005.
[39] Xie, Y., Pan, T., Lei, Q., Chen, C., Dong, X., Yuan, Y., Shen, J., Cai, Y., Zhou, C., Pinnau, I., Han, Y., 2021. Ionic Functionalization of Multivariate Covalent Organic Frameworks to Achieve an Exceptionally High Iodine-Capture Capacity. Angew Chem Int Ed 60, 22432–22440. https://doi.org/10.1002/anie.202108522.
[40] Xiong, X.H., Yu, Z.W., Gong, L.L., Tao, Y., Gao, Z., Wang, L., Yin, W.H., Yang, L.X., Luo, F., 2019. Ammoniating covalent organic framework (COF) for high-performance and selective extraction of toxic and radioactive uranium ions. Adv Sci 6, 1900547. https://doi.org/10.1002/advs.201900547.
[41] Xu, M., Wang, J., Zhang, L., Wang, Q., Liu, W., An, Y., Hao, L., Wang, C., Wang, Z., Wu, Q., 2022. Construction of hydrophilic hypercrosslinked polymer based on natural kaempferol for highly effective extraction of 5-nitroimidazoles in environmental water, honey and fish samples. J Hazard Mater 429, 128288. https://doi.org/10.1016/j.jhazmat.2022.128288.
[42] Xu, X., Gao, J., Zhang, Y., Zhang, L., 2023. Tailored novel multifunctional benzyl-functionalized magnetic ionic liquid for rapid and efficient monitoring of trace fluoroquinolones in food samples. Food Chem 404, 134654. https://doi.org/10.1016/j.foodchem.2022.134654.
[43] Ye, Y., Wu, T., Jiang, X., Cao, J., Ling, X., Mei, Q., Chen, H., Han, D., Xu, J.J., Shen, Y., 2020. Portable Smartphone-Based QDs for the Visual Onsite Monitoring of Fluoroquinolone Antibiotics in Actual Food and Environmental Samples. ACS Appl Mater Interfaces 12, 14552–14562. https://doi.org/10.1021/acsami.9b23167.
[44] Yu, K., Yue, M.E., Xu, J., Jiang, T.F., 2020. Determination of fluoroquinolones in milk, honey and water samples by salting out-assisted dispersive liquid-liquid microextraction based on deep eutectic solvent combined with MECC. Food Chem 332, 127371. https://doi.org/10.1016/j.foodchem.2020.127371.
[45] Yuan, Y., Yang, Y., Ma, X., Meng, Q., Wang, L., Zhao, S., Zhu, G., 2018. Molecularly imprinted porous aromatic frameworks and their composite components for selective extraction of uranium ions. Adv Mater 30, e1706507. https://doi.org/10.1002/adma.201706507.
[46] Yuan, Y., Yang, Y., Zhu, G., 2020. Molecularly imprinted porous aromatic frameworks for molecular recognition. ACS Cent Sci 6, 1082–1094. https://doi.org/10.1021/acscentsci.0c00311.
[47] Yusran, Y., Guan, X., Li, H., Fang, Q., Qiu, S., 2020. Postsynthetic functionalization of covalent organic frameworks. Natl Sci Rev 7, 170–190. https://doi.org/10.1093/nsr/nwz122.
[48] Zhang, B., Wei, M., Mao, H., Pei, X., Alshmimri, S.A., Reimer, J.A., Yaghi, O.M., 2018. Crystalline dioxin-linked covalent organic frameworks from irreversible reactions. J Am Chem Soc 140, 12715–12719. https://doi.org/10.1021/jacs.8b08374.
[49] Zhang, Q., Zhang, M., Huang, Z., Sun, Y., Ye, L., 2023. Molecularly imprinted polymers for targeting lipopolysaccharides and photothermal inactivation of pseudomonas aeruginosa. ACS Appl Polym Mater 5, 3055–3064. https://doi.org/10.1021/acsapm.3c00204.
[50] Zhang, Y., Ren, J., Yang, Z., Ma, Y., Zhang, Q., Zhang, B., 2021. Fabrication of surface-imprinted magnetic wrinkled microspheres and their specific adsorption of BSA. Ind Eng Chem Res 60, 11277–11288. https://doi.org/10.1021/acs.iecr.1c01803.
[51] Zhang, Z., Liu, Y., Huang, P., Wu, F.Y., Ma, L., 2021. Polydopamine molecularly imprinted polymer coated on a biomimetic iron-based metal-organic framework for highly selective fluorescence detection of metronidazole. Talanta 232, 122411. https://doi.org/10.1016/j.talanta.2021.122411.
[52] Zhao, M., Huang, S., Xie, H., Wang, J., Zhao, X., Li, M., Zhao, M., 2020. Construction of specific and reversible nanoreceptors for proteins via sequential surface-imprinting strategy. Anal Chem 92, 10540–10547. https://doi.org/10.1021/acs.analchem.0c01366.
[53] Zhao, Z., Liang, B., Wang, M., Yang, Q., Su, M., Liang, S.-X., 2022. Microporous carbon derived from hydroxyl functionalized organic network for efficient adsorption of flumequine: Adsorption mechanism and application potentials. Chem Eng J 427, 130943. https://doi.org/10.1016/j.cej.2021.130943.
[54] Zheng, J., Wahiduzzaman, M., Barpaga, D., Trump, B.A., Gutierrez, O.Y., Thallapally, P., Ma, S., McGrail, B.P., Maurin, G., Motkuri, R.K., 2021. Porous covalent organic polymers for efficient fluorocarbon-based adsorption cooling. Angew Chem Int Ed 60, 18037–18043. https://doi.org/10.1002/anie.202102337.
[55] Zhu, R., Zhang, P., Zhang, X., Yang, M., Zhao, R., Liu, W., Li, Z., 2022. Fabrication of synergistic sites on an oxygen-rich covalent organic framework for efficient removal of Cd(II) and Pb(II) from water. J Hazard Mater 424, 127301. https://doi.org/10.1016/j.jhazmat.2021.127301.